magnetochemistry

MDPI

Article

Novel Linear Trinuclear Cu^{II} Compound with Trapped Chiral Hemiaminal Ligand: Magnetostructural Study

Carlos Cruz [1,2,*], Nathalie Audebrand [3], Dayán Páez-Hernández [4] and Verónica Paredes-García [1,2,*]

[1] Departamento de Ciencias Químicas, Facultad de Ciencias Exactas, Universidad Andres Bello, Santiago 8370146, Chile
[2] Center for the Development of Nanoscience and Nanotechnology (CEDENNA), Santiago 9170022, Chile
[3] Univ Rennes, CNRS, INSA Rennes, ISCR (Institut des Sciences Chimiques de Rennes)—UMR 6226, F-35000 Rennes, France; nathalie.audebrand@univ-rennes.fr
[4] Center of Applied Nanosciences (CANS), Universidad Andres Bello, Santiago 8370146, Chile; dayan.paez@unab.cl
* Correspondence: c.cruzherrera@uandresbello.edu (C.C.); vparedes@unab.cl (V.P.-G.)

Abstract: A new trinuclear Cu^{II} compound $\{[Cu_3(HL')_2(H_2O)_2](ClO_4)_4\}\cdot(H_2O)_4$ (**1**) was obtained and presented a trapped chiral hemiaminal ($HL_{2'}$ = [(5-amino-4H-1,2,4-triazol-3-yl)amino](1H-imidazol-4-yl)methanol)). Compound **1** shows an almost flat cationic structure $[Cu_3(HL')_2(H_2O)_2]^{4+}$ with a Cu_3 linear core reached by the double Cu-OR/NN-Cu triazole/alkoxo bridge of the hemiaminal molecule. The Cu^{II} spin carriers are antiferromagnetically coupled, presenting a spin doublet ground state (S = 1/2) with a magnetic coupling constant of -179 cm^{-1}. Moreover, DTF calculations show that the planarity of the compound permits a sigma-type overlapping between the unpaired electrons of the spin carriers and the *p*-type orbitals of the coordinated N and O atoms producing an electronic delocalization through the bridging ligand responsible for the strong antiferromagnetic interactions observed experimentally.

Keywords: coordination compound; molecular magnetism; copper; hemiaminal

Citation: Cruz, C.; Audebrand, N.; Páez-Hernández, D.; Paredes-García, V. Novel Linear Trinuclear Cu^{II} Compound with Trapped Chiral Hemiaminal Ligand: Magnetostructural Study. *Magnetochemistry* **2023**, *9*, 175. https://doi.org/10.3390/magnetochemistry9070175

Academic Editor: Salah Massoud

Received: 22 May 2023
Revised: 22 June 2023
Accepted: 1 July 2023
Published: 6 July 2023

1. Introduction

Polynuclear molecular complexes containing copper(II) cations are characterized as having various structures and functions explored in fields such as chemistry, biochemistry, and materials science [1–7]. Also, different designs and arrangements of the Cu^{II} cations have been studied for their potential use in catalytic reactions involving oxidation or reduction and in developing new magnetic materials [1,2,4,8]. The isotropic spin state and coordination plasticity make this cation a useful spin carrier for magnetostructural correlations. Several copper(II) compounds with different dimensional structures and magnetic behaviors involving single-molecule magnets (SMMs) and single-chain magnets (SCMs) have been reported in the past years [9–13]. The effect of different bridging ligands on magnetic coupling has been explored in many cases using the concept of complementarity/counter-complementarity between the ligand and metal orbitals [14–17]. Azido and carboxylate are among the most common bridges in these compounds because of their diversity in bridging modes and efficiency in magnetic coupling. On the other hand, metal complexes involving Schiff bases containing N and O donors are particularly interesting as chelating and bridging ligands and have been central in developing coordination chemistry and molecular magnetism [18–22].

Triazole has also been widely studied in the molecular magnetism field [23,24], principally because this ligand can act as a nucleating linker, providing high versatility in preparing polynuclear coordination materials [25,26]. Moreover, triazole Schiff bases prepared using *o*-vanillin [27], quinoline [28], and acetic anhydride [29–31] have been a handful

as they have multiple N-donor centers and effective bridging capabilities to obtain polynuclear structures with interesting magnetic properties. Nevertheless, Schiff bases containing two different azoles are somewhat scarce, and only a few examples can be found with Fe^{II} and Fe^{III}-Co^{II} spin carriers [32,33], in which the azole Schiff bases are innocent in their magnetic properties.

Therefore, based on the remarkable coordination capabilities of triazole and the fact that multiple azole Schiff bases remain unexplored, the condensation of amino-triazoles with imidazole carbaldehyde can offer an attractive way to obtain new ligands capable of binding multiple metal cations and finding correlations between structure and magnetism, which is necessary for the design of new materials. The present work is focused on synthesizing, characterizing, and studying the magnetic properties of a new linear trinuclear copper(II) complex by combining single-crystal X-ray diffraction, magnetic susceptibility measurements, and DFT theoretical calculations.

2. Experimental

The precursors and solvents used to obtain the H_2L ligand were of p.a. quality (Sigma-Aldrich-Merck, Santiago, Chile) and were used without any previous purification. Also, the metallic salt used to obtain **1** complex was of p.a. quality. The quantitative content of C, H, and N was obtained on a Thermos CHNS Flash 2000 elemental analyzer using a solid crystalline sample. Thermogravimetric analyses were performed in an alumina holder and heated under an N_2 atmosphere from room temperature to 900 °C with a heating rate of 5 °C/min on a Mettler Toledo TGA/DSC-II system. Fourier transform infrared spectra were recorded on an ATR-FTIR-4000 Jasco in the 4000−400 cm^{-1} range without using any support.

2.1. Synthesis of Compound H_2L

The ligand H_2L was obtained by the condensation reaction of 4H-1,2,4-triazole-3,5-diamine and 1H-imidazole-4-carbaldehyde in a molar ratio of 1:1.

A mixture of 5 mmol of 1H-1,2,4-triazole-3,5-diamine (datrz) was dissolved in 10 mL of methanol (MeOH). Then, 10 mL methanolic solution of 5 mmol of 1H-imidazole-4-carbaldehyde (imcar) was added. After 10 min of reflux, the solution turned light yellow. Finally, after 3 h of reaction, the yellow precipitate of H_2L was separated by filtration and washed with MeOH. MW H_2L: 177.74 g/mol, yield 89%, based on datrz. Anal. Calc. for $C_6H_7N_7$: C, 40.87, H, 3.97, N, 55.16; Found, C, 41,70; H, 4.10; N, 56.10. FTIR: $\overline{\nu}$ C=N = 1670 cm^{-1}.

2.2. Synthesis of Compound {$[Cu_3(HL')_2(H_2O)_2](ClO_4)_4$}·$(H_2O)_4$ (1)

Caution: Perchlorate salts of transition metals have the potential to be explosive and should be handled with care. To a suspension of 0.35 mmol of HL_2 in 5 mL of MeOH under constant stirring, a clear blue solution of 0.5 mmol of $Cu(ClO_4)_2 \cdot 6H_2O$ was added. The suspension turned clear and changed to deep green. After 30 min of stirring, the solution was left undisturbed for crystallization. After two months, blue board crystals of $\{[Cu_3(HL')_2(H_2O)_2](ClO_4)_4\} \cdot 4H_2O$ (**1**) appeared. The crystalline product was separated by filtration and washed carefully to avoid dissolving the crystals. MW: 1085.91 g/mol. The yield is 55%, based on copper salt. Anal. Calc. for $C_{12}H_{28}Cl_4Cu_3N_{14}O_{24}$: C, 13.4, H, 2.6, N, 18.1; Found, C, 14.1; H, 2.4; N, 18.9. FTIR: $\overline{\nu}_{ClO4}$ = 1056 cm^{-1} (Figure S1). TGA: Thermogravimetric analysis of 1 indicates a weight loss of ~7% until 120 °C, associated with releasing crystallization water molecules (~6%). The weight remains unchanged until 220 °C, indicating that **1** is stable until this temperature. At 220 °C, the decomposition of **1** starts (Figure S2).

The trinuclear complex is very soluble in the most common organic solvents, such as methanol, ethanol, acetonitrile, dimethylformamide, tetrahydrofuran, and dimethyl sulfoxide. Efforts to speed up the crystallization of **1** using different crystallization techniques were unsuccessful. Only slow evaporation permits the formation of well-defined crystals of **1**.

2.3. X-ray Crystal Structure Analysis

Single crystals of **1** were directly picked up from the reaction media, immediately immersed in a drop of Paratone® oil, and mounted with a cryo-loop (Figure S3) on an APEXII Kappa-CCD Bruker AXS diffractometer equipped with a CMOS PHOTON 100 detector and using Mo-Kα radiation (λ = 0.71073 Å). The intensities were measured at 296 K. Frame integration and data reduction were carried out with the Bruker APEX2 program [34], and the SADABS program was employed for multiscan-type absorption corrections. Using the Olex2 [35] package, the crystal structures were solved with the ShelXT [36] structure solution program using Dual Methods and refined with the ShelXL [37] package using least-squares minimization based on F^2. Table 1 and Table S1 summarize the crystallographic data details on data collection and refinement parameters of the crystal structure. Structure drawings have been made with TOPOS software version 4.0 [38]. Additional data concerning the crystals and the refinement parameters are detailed in the supporting information. The structure was determined at room temperature, presenting one of the perchlorate anions with disorder and the four crystallization water molecules with high thermal agitation. These facts explain the obtained R-value.

Table 1. Crystal data and structure refinement for **1**.

Identification code	1
Empirical formula	$C_{12}H_{28}Cl_4Cu_3N_{14}O_{24}$ *
Formula weight	1085.9
Temperature/K	296
Crystal system	triclinic
Space group	P-1
a/Å	7.4052 (9)
b/Å	14.7151 (17)
c/Å	17.1455 (19)
α/°	110.303 (4)
β/°	100.416 (4)
γ/°	94.458 (4)
Volume/Å^3	1703.3 (3)
Z	2
ρ_{calc}g/cm^3	2.092
μ/mm^{-1}	2.284
F (000)	1066.0
Crystal size/mm^3	0.320 × 0.140 × 0.050
Radiation	MoKα (λ = 0.71073)
2Θ range for data collection/°	2.598 to 55.254
Index ranges	$-7 \leq h \leq 9$, $-19 \leq k \leq 18$, $-22 \leq l \leq 20$
Reflections collected	16,730
Independent reflections	7677 [R_{int} = 0.0629, R_{sigma} = 0.1129]
Data/restraints/parameters	7677/0/513
Goodness-of-fit on F^2	1.109
Final R indexes [I ≥ 2σ (I)]	R_1 = 0.0854, wR_2 = 0.2089
Final R indexes [all data]	R_1 = 0.1409, wR_2 = 0.2379
Largest diff. peak/hole/e Å^{-3}	1.61/−0.90

* 12 H atoms of the six water molecules were added to the final formula, $C_{12}H_{16}Cl_4Cu_3N_{14}O_{24}$.

The X-ray powder diffraction data were collected at room temperature on a PANalytical X'Pert MPD diffractometer with Cu K$\alpha_{1,2}$ radiation equipped with an X'celerator detector in the range of $4° < 2\theta < 50°$. The experimental X-ray powder diffraction patterns of the ground crystals agree with the theoretical patterns generated from the crystal structures. The indexing of the powder patterns has been recorded with the program DICVOL14 through the PreDICT interface [39]. The whole powder pattern fittings (pattern-matching with the Le Bail fit) were done employing the FULLPROF program [40] available in the software package WinPLOTR31 (2001) [41] (Figure S4). By fitting the powder pattern by pattern-matching with the Le Bail fit, it is possible to determine that the experimental XRPD

of **1** agrees with the calculated pattern generated by SC-XRD data, confirming that the single crystal structure well describes the diffracting species of powder samples.

2.4. Magnetic Measurement

Magnetic measurements were carried out using a Quantum Design Dynacool Physical Properties Measurement System (PPMS) equipped with a Vibrating Sample Magnetometer (VSM). The dc data were collected under an externally applied field of 10 kOe in the 1.8–300 K temperature range. Isothermal magnetization measurements were performed between 0 and 90 kOe at temperatures varying from 1.8 to 8 K. Diamagnetic corrections (estimated from Pascal constants) were considered [42].

2.5. Theoretical Calculations

All theoretical calculations were performed in the ORCA 5 program package [43] in the framework of density functional theory (geometry optimization and broken-symmetry calculations) and wave function base methods (local magnetic properties) [44–47]. Starting from the crystallographic data, the complex structure was prepared for the calculation by optimizing the hydrogen positions. Scalar relativistic effects were included via the Douglas-Kroll-Hess (DKH) Hamiltonian [48], and the hybrid-B3LYP functional combined with the def2-TZVPP basis set was used. The magnetic coupling calculations were performed in the broken symmetry (*BS*) approximation framework [45,49,50]. As recommended in the literature, a special integration, seven in this work, was used for the metals and atoms directly coordinated to paramagnetic centers. A large basis-set, def2-QZVPP, was used to describe Cu, N, and O atoms in the BS calculations [51]. The magnetic interaction between centers was evaluated by diamagnetic substitution, considering Cu-Cu pairs and replacing the third center with Zn as a diamagnetic atom. Considering these models, the magnetic coupling can be obtained by mapping the lowest triplet and singlet electronic states to the Heisenberg-Dirac-van Vleck Hamiltonian (HDvV) eigenstates. However, in the unrestricted DFT formalism, the singlet state would require a spin-adapted linear combination of more than one Slater determinant. Noodleman proposed a solution to this problem by converging a BS solution and mapping to the HDvV eigenstates using a spin-projection procedure. This work determined the *J* values from three different corrections of the spin-contaminated energies for the high-spin (*HS*) and broken-symmetry (*BS*) solutions [49–52].

$$J_a = \frac{2(E_{BS} - E_{HS})}{S_{HS}^2} \quad (1)$$

$$J_b = \frac{2(E_{BS} - E_{HS})}{S_{HS}(S_{HS} + 1)} \quad (2)$$

$$J_c = \frac{2(E_{BS} - E_{HS})}{< S^2 >_{HS} - < S^2 >_{BS}} \quad (3)$$

3. Results and Discussion

3.1. Synthetical Approach

The condensation of 1H-1,2,4-triazole-3,5-diamine (datrz) and 1H-imidazole-4-carbaldehyde (imcar) yields the imine H_2L as the main product (Scheme 1), corroborated by elemental analysis and FTIR, which also shows the absence of C=O absorption in the H_2L spectrum due to the formation of the C=N bond as a product of the condensation reaction. Nevertheless, as discussed in the structural characterization, the H_2L ligand is in **1** as a hemiaminal form, H_2L' (Figure S1b).

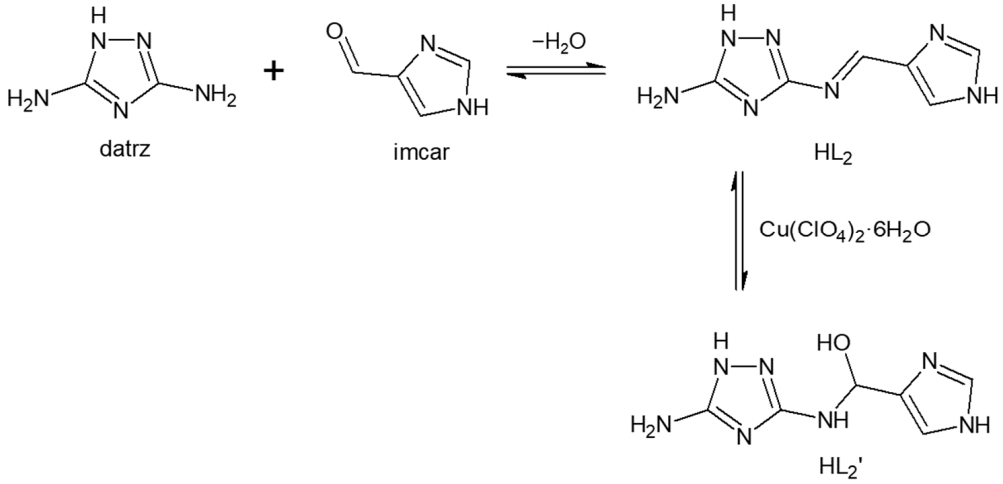

Scheme 1. Proposed synthetic route for ligand H_2L' = [(5-amino-1H-1,2,4-triazole-3-yl)amino] (1H-imidazol-4-yl)methanol; datrz = 1H-1,2,4-triazole-3,5-diamine, Imcar = 1H-imidazole-4-carbaldehyde, H_2L = 3-{(E)-[(1H-imidazol-4-yl)methylidene]amino}-1H-1,2,4-triazol-5-amine.

The Schiff base H_2L is insoluble in organic solvents such as methanol, ethanol, acetonitrile, dimethylformamide, tetrahydrofuran, and dimethyl sulfoxide. But when a methanolic suspension of H_2L is mixed with the methanolic solution of Cu^{II} salt, the suspension turns immediately into a deep, clear green solution. The synthesis of **1** can be explained based on the equilibrium between H_2L and H_2L' shown in Scheme 1.

When the solution of $Cu(ClO_4)_2 \cdot 6H_2O$ is added to the suspension of H_2L, the presence of water molecules probably displaces the equilibrium toward H_2L', the hydrolyzed form of H_2L. The hemiaminal ligand H_2L' was also stabilized by coordinating to copper(II) cations, thus explaining the presence of H_2L', the hemiaminal intermediate (carbinolamine), in **1**.

3.2. Description of the Crystal Structure

Compound **1** crystallizes in a triclinic $P\bar{1}$ space group. The asymmetric unit comprises three Cu^{II} centers, two monoprotonated HL'^{-} ligand units, and two water molecules, forming a discrete complex. Additionally, four perchlorate anions and four H_2O solvate molecules are found in the crystal packing.

The structure of complex **1** consists of a molecular pseudo-flat complex with the two organic ligands coordinating the three Cu^{II} central cations and forming a linear $[Cu_3(HL')_2(H_2O)_2]^{4+}$ trinuclear unit (Figure 1). The geometry of the three copper cations is square planar, with a trans-CuN_2O_2 environment in each center. The Cu2 in the middle presents two κN,O-HL'^{-} ligands coordinated by one N of the triazole and the alkoxo group, thus forming a six-membered chelating ring.

Meanwhile, in the external copper cations, Cu1 and Cu3, the CuN_2O_2 environment is reached by the κN′, HL'^{-} coordination modes of both ligands, belonging in one case to the imidazole ring and in the other to the triazole ring. The κO,N″ coordination mode of -HL'^{-} permits the alkoxo groups to act as μ_2-bridges in **1**. Likewise, both metal cations have a coordinated H_2O molecule that completes a tetra-coordinated environment around Cu1 and Cu3. In this way, HL'^{-} ligands behave as tris-tetradentate linkers that bridge the central Cu2 with Cu1 and Cu3 by two triazole/alkoxo bridges at the same time, with Cu···Cu distances of Cu1···Cu2 = 3.3635 (14) Å and Cu2 ··· Cu3 = 3.3284 (14) Å (Table 2).

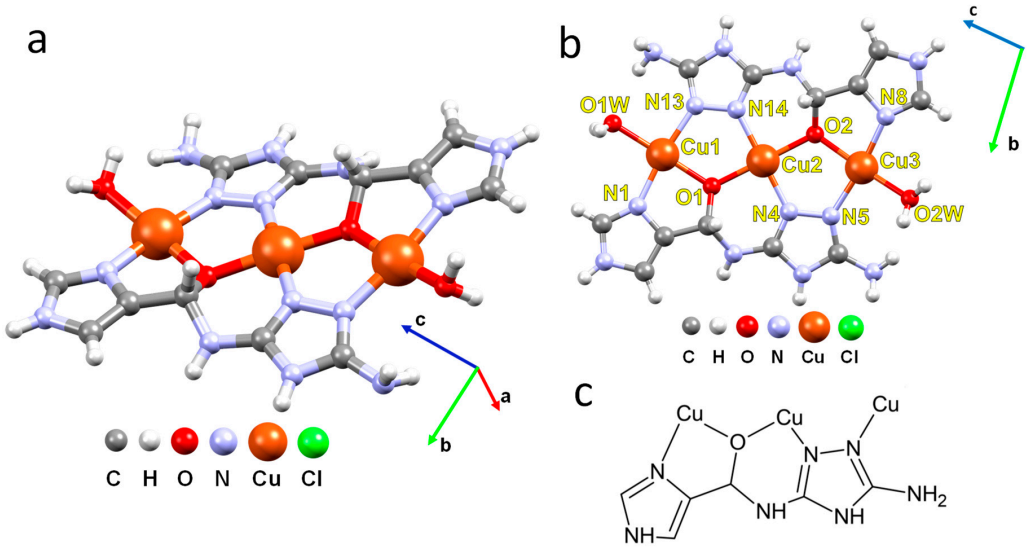

Figure 1. (**a**) Trinuclear linear structure $[Cu_3(HL')_2(H_2O)_2]^{4+}$ of 1; (**b**) numeration of core atoms in 1; and (**c**) coordination mode of HL'^{-}.

Table 2. Cu-O and Cu-N bond length in compound **1**.

Cu-O Bond Length (Å)			Cu-N Bond Length (Å)			Cu-Cu Distances (Å)		
Cu1	O1	1.960 (6)	Cu1	N1	1.939 (7)	Cu1	Cu2	3.3635 (14)
Cu2	O1	1.915 (5)	Cu1	N13	1.979 (7)	Cu2	Cu3	3.3284 (14)
Cu2	O2	1.955 (5)	Cu2	N4	1.921 (7)	Cu1	Cu1[1]	7.4052 (9)
Cu3	O2	1.957 (5)	Cu2	N14	1.939 (7)	Cu2	Cu2[1]	7.4052 (9)
Cu1	O1W	1.991 (6)	Cu3	N5	1.966 (7)	Cu2	Cu3[1]	7.3084 (17)
Cu3	O2W	2.002 (6)	Cu3	N8	1.946 (7)			
Cu1	O12	2.514 (9)						
Cu1 [1]	O14	2.660 (8)						
Cu2	O3	2.669 (7)						
Cu2	O5[1]	2.747(8)						
Cu3	O6	2.617(9)						
Cu3	O9	2.510(9)						

[1] x+1, y, z.

Furthermore, although HL'^{-} presents two rigid triazole and imidazole groups, the ligand is not perfectly flat because the sp^3 hybridization in the carbons C4 and C10 connects both heterocyclic fragments. Then, C4* and C10* atoms are stereogenic centers of each HL'^{-} ligand, presenting an L/D-configuration. In this sense, the hydrolyzation of H_2L gives rise to a chiral HL'^{-} hemiaminal ligand, each $[Cu_3(HL')_2(H_2O)_2]^{4+}$ unit composed of a unique configuration of L- or D-HL'^{-} ligand (Figure 2a). Figure 2b shows a view of the *ab* plane, in which it is possible to observe that the $[Cu_3(HL')_2(H_2O)_2]^{4+}$ complexes in the unit cell are related to each other by an inversion center; thus compound **1** is crystallizing as a racemic mixture. Hemiaminal ethers have been obtained in coordination compounds through the hydrolysis of imine ligands by adding alcohol molecules such as methanol [53]. However, the addition of water is somewhat less common. In this sense, HL'^{-} can be considered as a trapped deprotonated form of the unstable hemiaminal derivative of H_2L [54], stabilized by coordination to an acidic metal center and the templating effect due to the coordination to copper cations.

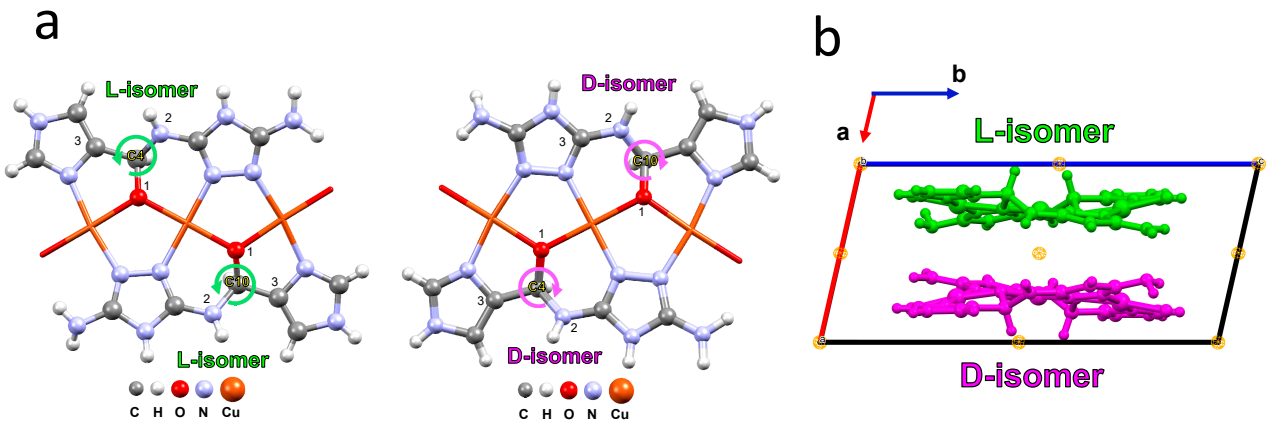

Figure 2. (**a**) L and D isomers of the HL'^{-} ligand showing the tetrahedral geometry of C4* and C10* stereogenic centers. (**b**) View of the inversion center through *ab* plane.

The sp^3 hybridization of C4*/C10* also affects the overall geometry of the complex. A side view of the Cu_3 central core shows that the three Cu^{II} cations are not perfectly aligned. This is mainly due to the tetrahedral geometry of C4*/C10* carbons in the -NC*- moiety connecting the imidazole and triazole rings (Figure 2b), which bends the whole structure of the complex, as evidenced by a large -CNC*C- torsion angle (179.5 (8)° for C4* and 177.9 (7)° for C10). Furthermore, considering the planes containing each CuN_2O_2 labeled as Cu1, Cu2, and Cu3 (Figure S5), it is observed that the central $Cu2N_2O_2$ moiety is aligned more planarly with $Cu1N_2O_2$ (8.19° interplanar angle) than $Cu3N_2O_2$ (18.13° interplanar angle).

Furthermore, compound **1** presents four perchlorate molecules balancing the charge of the $[Cu_3(HL')_2(H_2O)_2]^{4+}$ complex, presenting a packing through the axis with layers of $[Cu_3(HL')_2(H_2O)_2]^{4+}$ trinuclear units and three ClO_4^- anions interacting through the axial zones of the square planar cations, with $Cu\cdots O_{perchorate}$ distances ranging between 2.510 (9) and 2.747 (8) Å (Figure 3). This packing has been observed in another planar-shaped polynuclear Cu^{II} compound with rigid triazole-based ligands [55]. In this case, Cu-O is shorter (less than 2.5 Å considered formally as a bond), and the packing is described as a 1D polymer rather than an anionic complex.

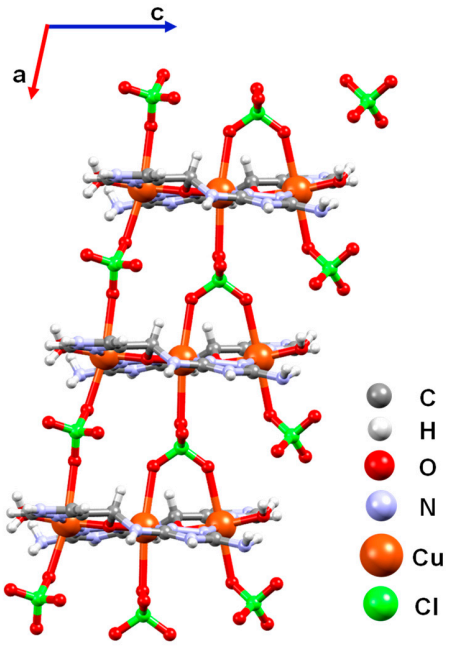

Figure 3. Anionic packing through *ac* axis.

3.3. Magnetic Properties

The magnetic measurements were performed using a polycrystalline powder sample. Figure 4 shows the $\chi_m T$ vs. T plot for 3–1.8 K at 10 kOe for compound **1**, where χ_m is the molar magnetic susceptibility per Cu_3 unit. At room temperature, the $\chi_m T$, 0.57 emu K mol^{-1}, is smaller than expected for three uncoupled Cu^{II} spin carriers (1.125 emu K mol^{-1} for S = 1/2 and g = 2.0). By lowering the temperature, the $\chi_m T$ product gradually decreases, reaching a value of 0.37 emu K mol^{-1} near 100 K (the expected value for a strongly coupled Cu_3 complex with S = 1/2), indicative that antiferromagnetic interactions are present in **1**. From this point, a constant value of the $\chi_m T$ is observed until approximately 10 K. Then, a slight decrease in the $\chi_m T$ is observed, reaching a value of 0.33 emu K mol^{-1} at 1.8 K. The presence of the plateau below 100 K means that antiferromagnetic interactions between the central (Cu2) and terminal (Cu1 and Cu3) copper centers lead to an overall doublet spin ground state (S = 1/2).

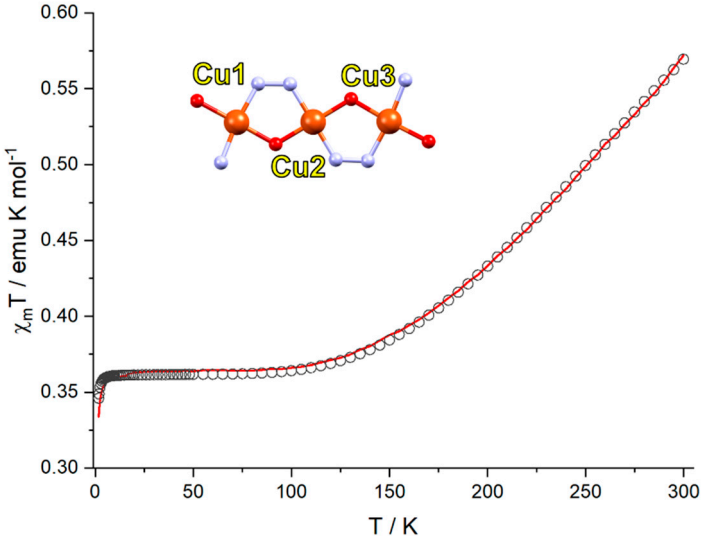

Figure 4. $\chi_m T$ vs. T plot at 10 kOe; the red line represents the fitting using the trinuclear model of $\hat{H}_1$ and $\hat{H}_2$. M_{red} vs. H plots at 1.8, 3, 5, and 8 K.

Additionally, the field dependence of magnetization at 1.8, 3, 5, and 8 K, represented as reduced magnetization (M_{red}) against applied field H is shown in Figure S6. At 1.8 K, the magnetization reaches a saturation value of 1.1 μ_β at 90 kOe. This is also consistent with the $\chi_m T$ values observed below 100 K that correlate well with a single unpaired electron, thus corroborating the antiferromagnetic coupling between the spin carriers and essentially a doublet spin ground state at low temperature.

As shown in the structural section, **1** shows a molecular structure consisting of a central core with a linear arrangement of three copper cations (Cu1-Cu2-Cu3) connected by an N,N-triazole and an O-alkoxo bridge with Cu1···Cu2 = 3.3635 (14) Å and Cu2···Cu3 = 3.3284 (14) Å intramolecular distances. In this sense, the magnetic interactions can be modeled using an isotropic spin Hamiltonian comprising the interaction of three centers of S = 1/2 (Cu1, Cu2, and Cu3) through two magnetic pathways:

$$\hat{H}_1 = -J_1(S_{Cu1}S_{Cu2} - S_{Cu2}S_{Cu3}) \quad (4)$$

where J_1 is the magnetic interaction constant between Cu1–Cu2 and Cu2–Cu3. Using this spin Hamiltonian, a fit of magnetic data was performed using PHI software (2003) [56]. The best-fit parameters are $J_1 = -179$ cm^{-1} considering $g_{Cu1} = g_{Cu3} = 2.02$ and $g_{Cu2} = 2.2$ (residual as implemented in PHI, $R = 0.28$).

As mentioned, the central Cu3 moiety is bridged by two chemical connectivities: a Cu-NN-Cu triazole bridge and a Cu-OR-Cu alkoxo bridge (Cu-OR/NN-Cu Figure S7).

Separately, it has been reported that the NN bridge belonging to pyrazole, pyrazine, or hydrazine mediates antiferromagnetic (AFM) couplings between Cu^{II} centers, with the magnitude of the interaction strongly dependent on the Cu-NN-Cu torsion angle [57]. Meanwhile, the magnetic interaction through oxo bridges belonging to hydroxo, alkoxo, or phenoxo strongly depends on the Cu-O-Cu angle, mediating either ferro- or antiferromagnetic interactions [58]. However, other structural and bonding features, such as the planarity of the Cu-O-Cu moiety, should be considered for a complete magnetostructural relationship.

A careful search in the crystallographic data yeilded seven trinuclear compounds that share the same linear Cu_3 core with two Cu-OR/NN-Cu bridges (Table 3). AFM couplings are observed for all reported compounds and are also characterized by Cu-O-Cu angles between ~115–120° and Cu-NN-Cu torsion angles in a broader range (~7–40°). Dogaheh et al. [59] reported a compound bearing a Cu–OR/NN–Cu moiety formed by a hydrazine/phenoxy bridge belonging to hydrazine-Schiff base ligands. The authors conclude a general trend in the Cu–OR/NN–Cu arrangement: a similar Cu-O-Cu bite angle around 115° is observed in all the Cu-OR/NN-Cu, consistent with the observed Cu_3 compounds of Table 3. Moreover, the authors conclude that the larger the Cu-NN-Cu bridging moiety, the weaker the AFM coupling between the Cu^{II} cations. According to the compound reported by the authors, a -7.21 cm^{-1} coupling is observed for a 35.9° torsion angle. Nevertheless, the trend does not seem to match the trinuclear family reported by Adhikary et al. with the same hydrazine NN bridge [60]. The authors provide torsion angles ranging from ~29 to ~40°, obtaining -113.1 cm^{-1} for the lesser angle, and -249.7 cm^{-1} for the greater. In the case of compound **1**, a coupling constant of -179 cm^{-1} is obtained with a lower Cu-NN-Cu angle of 17.2 (8)/13.7 (8)°. In this sense, Bazhina et al. [20] reported a coupling of $-149/-175$ cm^{-1} with a much lesser Cu-NN-Cu angle of 6.9 (8)°/8.0 (8)° with a NN moiety belonging to triazole rings the same as **1**. Evidently, the Cu-NN-Cu and Cu-O-Cu angles, as structural parameters, are insufficient to analyze magnetic properties in this trinuclear compound. More subtle features affecting delicate orbital overlapping must be considered for an accurate magnetostructural analysis.

Table 3. Related trinuclear lineal Cu^{II}-based compounds with Cu-OR/NN-Cu bridges.

Compound	Cu-NN-Cu [a]	Cu-O-Cu [b]	J (cm^{-1})	Ref.
$[Cu_3(HYDRAV)_2Cl_2]$ [c]	35.9	115	−7.21	[59]
$[Cu_3L_2(BF_4)(H_2O)_2](BF_4)$ [d]	40.5 (2)/33.0 (1)	116.23 (7)/118.40 (7)	−170	[60]
$[Cu_3L_2(NO_3)_2(H_2O)_2](H_2O)_3$ [d]	28.86	116.95	−113.1	[60]
$[Cu_3L_2(Cl)_2(CH_3OH)_2](H_2O)_2$ [d]	30.54	116.89	−98.3	[60]
$[Cu_3L_2(ClO4)_2(H2O)_2]$ [d]	40.19/28.92	117.67/117.91	−249.7	[60]
$\{[Cu_3L^1(L^2)_2(NO_3)_2(H_2O)_2](NO_3)\cdot 1.5H_2O\}_n$ [e]	−6.9 (8)/8.0 (8)	119.3 (3)/124.5 (3)	−149/−175	[20]
$Cu_3(L^3)_2(OH)_2(H_2O)_2$ [f]	13.1	124.2	-	[61]
$\{[Cu_3(HL')_2(H_2O)_2](ClO_4)_4\}\cdot(H_2O)_4$	17.2 (8)/13.7 (8)	120.5 (3)/116.6 (3)	−179	*

[a] torsion angle (°). [b] bond angle (°). [c] $HYDRAV_2$ = Schiff base made with 1-(hydrazineylidenemethyl)naphthalen-2-ol, o-vanillin and (2-hydroxy-3-methoxybenzaldehyde). [d] H_2L = 6,6-((1E,10E)-hydrazine-1,2-diylidenebis(methanylylidene))bis(2-methoxyphenol). [e] H_2L^1 = 4-[bis(pyridin-2-yl-methanol)]amino-1,2,4-triazole; L^2= 4-amino-4H-1,2,4-triazole; the authors also reports an additional zJ of -0.7 cm^{-1}. [f] L^3 = (5-bis(5-tetrazolo)-3-thiapentane. AFM interactions are reported as θ = 240.77 K. * this work.

3.4. Theoretical Calculations

The theoretical study of the complex using DFT calculations considering the broken-symmetry approach allowed, firstly, to corroborate an antiferromagnetic coupling between the metal centers resulting in a doublet (S = 1/2) as a molecular ground state. The minimum energy configuration found (540 cm^{-1} more stable than the high spin S = 3/2 configuration) shows that Cu2 is coupled to the terminal copper cations in the ground state. The local planar square symmetry around each metal justifies that at each center, the unpaired electron is in an orbital that allows a sigma-type to overlap with the *p*-type orbitals of the coordinated N and O. This means that the magnetic coupling is mainly due to the electronic

delocalization through the bridging ligand, which in turn, as previously discussed, is closely related to the torsion experienced in the Cu_3 core.

From the structural information obtained for the complex, where the Cu1···Cu3 distance is 6.683 Å, it is possible to propose a weak coupling between the terminal Cu cations (Cu1–Cu3). For this reason, the proposed spin Hamiltonian (Equation (4)) only considers the interaction between neighboring atoms. A J_3, representing the magnetic coupling between terminal centers, was also calculated to validate this approach. In this case, the central Cu2 was substituted by Zn. Table 4 summarizes the obtained results. As observed experimentally, the calculations predict a strong coupling between neighboring coppers, while the Cu1–Cu3 interaction could be neglected, given the low value of the calculated coupling constant. It is important to remember that this type of calculation tends to overestimate the coupling constant values. Therefore, for this work, this study is not intended to be quantitative but to provide additional magnetostructural information [62]. An important detail to note is that the values of J_a and J_c have excellent agreement with the strong coupling limit for this system. Theoretically, this means that both *HS* and *BS* states are well represented at the level of theory, and a non-projected spin scheme could be a good approximation in this case. From a structural point of view, this means that the α and β spins are being covalently shared and not localized on the spin carriers [49–52].

Table 4. Calculated magnetic coupling constants (J in cm^{-1}) and Mulliken atomic spin populations on the atoms that directly connect the metals for high-spin (*HS*) and broken-symmetry (*BS*) configurations.

	Cu1–Cu2 (J_1)	**Cu2–Cu3 (J_2)**	**Cu1–Cu3 (J_3)**
J_a	−349.3	−207.7	−8.8
J_b	−174.6	−103.8	−4.4
J_c	−337.8	−202.9	−8.8
$\Delta\rho_{HS}$ (Cu)	0.680 0.701	0.679 0.698	0.689 0.690
$\Delta\rho_{BS}$ (Cu)	−0.665 0.686	−0.669 0.689	−0.689
$\Delta\rho_{HS}$ (O)	0.172	0.175	
$\Delta\rho_{BS}$ (O)	0.021	0.019	
$\Delta\rho_{HS}$ (N)	0.045 0.052	0.043 0.059	
$\Delta\rho_{BS}$ (N)	−0.052 0.057	−0.056 0.052	

Figure 5 shows the spin density maps obtained from the diamagnetic substitution to obtain J_1, J_2, and J_3. These maps allow us to corroborate the electronic delocalization and how the covalent nature of the metal-ligand interaction is responsible for spin polarization on the atoms directly coordinated to the metal centers. The calculated spin densities show a reduction in the formal value ($\Delta\rho = 1$) on the copper atoms due to delocalization and a partial open shell on the N and O bridging atoms. The delocalization on the bridging O atom between two copper atoms is higher, as evidenced by its spin density value. In the BS configuration, the density drops practically to zero on this atom due to the balance between alpha and beta electron densities. On the other hand, the spin density on the NN moiety of the triazole fragments is small but non-negligible, corroborating that the spin polarization mechanism through the bonding strongly dominates the magnetic coupling in the Cu_3 core of this complex. In other words, the kinetic exchange directly related to electron delocalization plays a key role in the coupling mechanism. Its contribution to the J values is more significant than the direct exchange interaction [63]. This fact corroborates the fact that even the subtle structural characteristics must be considered for the magnetostructural analysis because the spin polarization is closely related to the delicate orbital overlapping between the spin carriers by the bridging ligands.

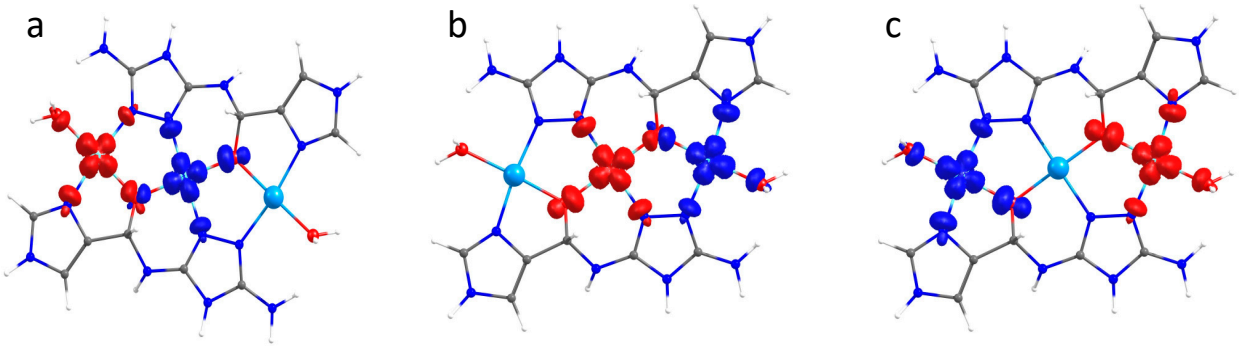

Figure 5. Spin density maps (isovalue = 10^{-5} a.u.) of the broken-symmetry states constructed to obtain J_1 (**a**), J_2 (**b**), and J_3 (**c**).

4. Conclusions

We have reported the synthesis and characterization of a new molecular compound, $\{[Cu_3(HL')_2(H_2O)_2](ClO_4)_4\}\cdot(H_2O)_4$, which has three paramagnetic copper(II) centers with a linear arrangement. The linear assembly of the spin carrier is reached by the coordination of the chiral hemiaminal form derived from the Schiff base obtained for the condensation reaction of 4H-1,2,4-triazole-3,5-diamine and 1H-imidazole-4-carbaldehyde. The hemiaminal bridges the copper cations through Cu-NN-Cu and alkoxo Cu-OR-Cu bridges. The trinuclear compound is dominated by antiferromagnetic interactions, presenting a doublet spin ground state (S = 1/2). Moreover, the planar square symmetry around each metal cation permits a sigma-type overlapping between the unpaired electrons of the spin carriers and the *p*-type orbitals of the coordinated N and O atoms, producing electronic delocalization through the bridging ligand and, therefore strong antiferromagnetic interactions.

Supplementary Materials: The following supporting information can be downloaded at: https://www.mdpi.com/article/10.3390/magnetochemistry9070175/s1, Figure S1: (a) Spectra of H2L ligand (black) diatrz (red) and 4carIm (blue). (b) Spectra of H2L (black) and of 1 (red); Figure S2: Thermogram in N2 atmosphere of compound 1; Figure S3: Le Bail fit of the X-ray powder diffraction patterns of powder sample of 1. The powder pattern fittings by pattern-matching with the Le Bail fit is possible to determine that the experimental XRPD of 1 agree with the calculated pattern generated by the SC-XRD data; Figure S4: (a) Crystal of 1 used for X-ray Crystal Structure Analysis and (b) bulk crystalline sample used for characterization; Figure S5: view of Cu1-Cu2-Cu3 linear core in compound 1; Cu1/Cu2 and Cu2/Cu3 planes; Figure S6. Isothermal magnetization at 1.8 (■), 3 (●), 5 (Δ) and 8 K (Δ) for 1; Figure S7. Atom label in Cu3 central core; Cu-NN-Cu torsion angles in Cu3 central core in 1; Table S1. Complete Data of refinement of 1. CCDC 2263971 contains the supplementary crystallographic data for this publication. These data can be obtained free of charge via www.ccdc.cam.ac.uk/data_request/cif, by emailing data_request@ccdc.cam.ac.uk, or by contacting The Cambridge Crystallographic Data Centre, 12 Union Road, Cambridge CB2 1EZ, UK; fax: +44 1223 336033.

Author Contributions: C.C. writing—original draft preparation, crystal structure, and magneto structural analysis; N.A. crystal structure analysis; D.P.-H. theoretical calculations; V.P.-G. writing—review and editing, magneto structural analysis. All authors have read and agreed to the published version of the manuscript.

Funding: This research was funded by ANID FONDECYT Postdoctorado N° 3210314 and ANID FONDECYT Regular N° 1211394.

Institutional Review Board Statement: Not applicable.

Informed Consent Statement: Not applicable.

Data Availability Statement: Data are available upon request to the corresponding authors.

Acknowledgments: The authors thank ANID FONDECYT Regular N°1211394, CONICYT-FONDEQUIP/PPMS/EQM130086-UNAB, the French-Chilean International Research Project "Cooperation in Inorganic Chemistry" (CoopIC), and Financiamiento Basal AFB220001 CEDENNA. C.C. acknowledges the financial support of ANID FONDECYT Postdoctorado N° 3210314. N.A. acknowledges T. Roisnel from CDIFX (Centre de Diffractométrie X), UMR CNRS 6226 Rennes, for single-crystal X-ray data collection.

Conflicts of Interest: The authors declare no conflict of interest.

References

1. De Han, S.; Zhao, J.P.; Liu, S.J.; Bu, X.H. Hydro(Solvo)Thermal Synthetic Strategy towards Azido/Formato-Mediated Molecular Magnetic Materials. *Coord. Chem. Rev.* **2015**, *289–290*, 32–48. [CrossRef]
2. Salvadeo, E.; Dubois, L.; Latour, J.M. Trinuclear Copper Complexes as Biological Mimics: Ligand Designs and Reactivities. *Coord. Chem. Rev.* **2018**, *374*, 345–375. [CrossRef]
3. Chen, Q.F.; Cheng, Z.Y.; Liao, R.Z.; Zhang, M.T. Bioinspired Trinuclear Copper Catalyst for Water Oxidation with a Turnover Frequency up to 20000 S-1. *J. Am. Chem. Soc.* **2021**, *143*, 19761–19768. [CrossRef] [PubMed]
4. Smits, N.W.G.; Rademaker, D.; Konovalov, A.I.; Siegler, M.A.; Hetterscheid, D.G.H. Influence of the Spatial Distribution of Copper Sites on the Selectivity of the Oxygen Reduction Reaction. *Dalt. Trans.* **2022**, *51*, 1206–1215. [CrossRef] [PubMed]
5. Muñoz-Becerra, K.; Zagal, J.H.; Venegas, R.; Recio, F.J. Strategies to Improve the Catalytic Activity and Stability of Bioinspired Cu Molecular Catalysts for the ORR. *Curr. Opin. Electrochem.* **2022**, *35*, 101035. [CrossRef]
6. Altowyan, M.S.; Khalil, S.M.S.M.; Al-Wahaib, D.; Barakat, A.; Soliman, S.M.; Ali, A.E.; Elbadawy, H.A. Synthesis of a Novel Unexpected Cu(II)–Thiazolidine Complex—X-Ray Structure, Hirshfeld Surface Analysis, and Biological Studies. *Molecules* **2022**, *27*, 4583. [CrossRef]
7. Pandolfo, L.; Pettinari, C. Trinuclear Copper(Ii) Pyrazolate Compounds: A Long Story of Serendipitous Discoveries and Rational Design. *CrystEngComm* **2017**, *19*, 1701–1720. [CrossRef]
8. Geer, A.M.; Musgrave, C.; Webber, C.; Nielsen, R.J.; McKeown, B.A.; Liu, C.; Schleker, P.P.M.; Jakes, P.; Jia, X.; Dickie, D.A.; et al. Electrocatalytic Water Oxidation by a Trinuclear Copper(II) Complex. *ACS Catal.* **2021**, *11*, 7223–7240. [CrossRef]
9. Kintzel, B.; Böhme, M.; Liu, J.; Burkhardt, A.; Mrozek, J.; Buchholz, A.; Ardavan, A.; Plass, W. Molecular Electronic Spin Qubits from a Spin-Frustrated Trinuclear Copper Complex. *Chem. Commun.* **2018**, *54*, 12934–12937. [CrossRef]
10. Rabelo, R.; Stiriba, S.E.; Cangussu, D.; Pereira, C.L.M.; Moliner, N.; Ruiz-García, R.; Cano, J.; Faus, J.; Journaux, Y.; Julve, M. When Molecular Magnetism Meets Supramolecular Chemistry: Multifunctional and Multiresponsive Dicopper(Ii) Metallacyclophanes as Proof-of-Concept for Single-Molecule Spintronics and Quantum Computing Technologies? *Magnetochemistry* **2020**, *6*, 69. [CrossRef]
11. Manzur, J.; Mora, H.; Vega, A.; Venegas-Yazigi, D.; Novak, M.A.; Sabino, J.R.; Paredes-García, V.; Spodine, E. Mononuclear and Polynuclear Copper(II) Complexes Derived from Pyridylalkylaminomethylphenol Polypodal Ligands. *Inorg. Chem.* **2009**, *48*, 8845–8855. [CrossRef] [PubMed]
12. Barros, W.P.; Da Silva, B.C.; Reis, N.V.; Pereira, C.L.M.; Doriguetto, A.C.; Cano, J.; Pirota, K.R.; Pedroso, E.F.; Julve, M.; Stumpf, H.O. Discrete Trinuclear Copper(Ii) Compounds as Building Blocks: The Influence of the Peripheral Substituents on the Magnetic Coupling in Oxamato-Bridged Complexes. *Dalt. Trans.* **2014**, *43*, 14586–14595. [CrossRef]
13. Grenda, S.; Beau, M.; Luneau, D. Synthesis, Crystal Structure and Magnetic Properties of a Trinuclear Copper(II) Complex Based on P-Cresol-Substituted Bis(α-Nitronyl Nitroxide) Biradical. *Molecules* **2022**, *27*, 3218. [CrossRef] [PubMed]
14. Nishida, Y.; Takeuchi, M.; Takahashi, K.; Kida, S. Preparation and Crystal Structure of a Binuclear Copper(II) Complex Bridged by an Alkoxo-Oxygen Atom an Acetate Ion. *Chem. Lett.* **1983**, *12*, 1815–1818. [CrossRef]
15. Nishida, Y.; Takeuchi, M.; Takahashi, K.; Kida, S. Orbital Complementary and Countercomplementary Effects in Superexchange Interaction through Heterobridges in Binuclear Copper(II) Complexes. *Chem. Lett.* **1985**, *14*, 631–634. [CrossRef]
16. McKee, V.; Zvagulis, M.; Dagdigian, J.V.; Patch, M.G.; Reed, C.A. Hemocyanin Models: Synthesis, Structure, and Magnetic Properties of a Binucleating Copper(II) System. *J. Am. Chem. Soc.* **1984**, *106*, 4765–4772. [CrossRef]
17. McKee, V.; Zvagulis, M.; Reed, C.A. Further Insight into Magnetostructural Correlations in Binuclear Copper(II) Species Related to Methemocyanin: X-Ray Crystal Structure of a 1,2-μ-Nitrito Complex. *Inorg. Chem.* **1985**, *24*, 2914–2919. [CrossRef]
18. Herrera, A.M.; Kalayda, G.V.; Disch, J.S.; Wikstrom, J.P.; Korendovych, I.V.; Staples, R.J.; Campana, C.F.; Nazarenko, A.Y.; Haas, T.E.; Rybak-Akimova, E.V. Reactions at the Azomethine C=N Bonds in the Nickel(II) and Copper(II) Complexes of Pyridine-Containing Schiff-Base Macrocyclic Ligands. *Dalt. Trans.* **2003**, 4482–4492. [CrossRef]
19. Yusuf, T.L.; Oladipo, S.D.; Zamisa, S.; Kumalo, H.M.; Lawal, I.A.; Lawal, M.M.; Mabuba, N. Design of New Schiff-Base Copper(II) Complexes: Synthesis, Crystal Structures, DFT Study, and Binding Potency toward Cytochrome P450 3A4. *ACS Omega* **2021**, *6*, 13704–13718. [CrossRef]
20. Bazhina, E.S.; Bovkunova, A.A.; Medved'ko, A.V.; Efimov, N.N.; Kiskin, M.A.; Eremenko, I.L. Unusual Polynuclear Copper(II) Complexes with a Schiff-Base Ligand Containing Pyridyl and 1,2,4-Triazolyl Rings. *J. Clust. Sci.* **2019**, *30*, 1267–1275. [CrossRef]
21. Biswas, C.; Drew, M.G.B.; Ruiz, E.; Estrader, M.; Diaz, C.; Ghosh, A. Synthesis, Crystal Structure and Magnetic Properties of Three Unprecedented Tri-Nuclear and One Very Rare Tetra-Nuclear Copper(Ii) Schiff-Base Complexes Supported by Mixed Azido/Phenoxo/Nitrato or Acetato Bridges. *Dalt. Trans.* **2010**, *39*, 7474–7484. [CrossRef]

22. Middya, P.; Roy, D.; Chattopadhyay, S. Synthesis, Structures and Magnetic Properties of End-on Pseudo-Halide Bridged Dinuclear Copper(II) Complexes with N,O-Donor Salicylaldimine Schiff Base Blocking Ligands: A Review. *Inorganica Chim. Acta* **2023**, *548*, 121377. [CrossRef]
23. Roubeau, O. Triazole-Based One-Dimensional Spin-Crossover Coordination Polymers. *Chem.–A Eur. J.* **2012**, *18*, 15230–15244. [CrossRef]
24. Klingele, M.H.; Brooker, S. The Coordination Chemistry of 4-Substituted 3,5-Di(2-Pyridyl)-4H-1,2,4-Triazoles and Related Ligands. *Coord. Chem. Rev.* **2003**, *241*, 119–132. [CrossRef]
25. Aromí, G.; Barrios, L.A.; Roubeau, O.; Gamez, P. Triazoles and Tetrazoles: Prime Ligands to Generate Remarkable Coordination Materials. *Coord. Chem. Rev.* **2011**, *255*, 485–546. [CrossRef]
26. Haasnoot, J.G. Mononuclear, Oligonuclear and Polynuclear Metal Coordination Compounds with 1,2,4-Triazole Derivatives as Ligands. *Coord. Chem. Rev.* **2000**, *200–202*, 131–185. [CrossRef]
27. Heras Ojea, M.J.; Hay, M.A.; Cioncoloni, G.; Craig, G.A.; Wilson, C.; Shiga, T.; Oshio, H.; Symes, M.D.; Murrie, M. Ligand-Directed Synthesis of {MnIII5} Twisted Bow-Ties. *Dalt. Trans.* **2017**, *46*, 11201–11207. [CrossRef] [PubMed]
28. Creaven, B.S.; Devereux, M.; Foltyn, A.; McClean, S.; Rosair, G.; Thangella, V.R.; Walsh, M. Quinolin-2(1H)-One-Triazole Derived Schiff Bases and Their Cu(II) and Zn(II) Complexes: Possible New Therapeutic Agents. *Polyhedron* **2010**, *29*, 813–822. [CrossRef]
29. Penkova, L.; Demeshko, S.; Haukka, M.; Pavlenko, V.A.; Meyer, F.; Fritsky, I.O. Bi- and Trinuclear Copper(II) Complexes with a Bridging Pyrazole/Oxime Ligand: Structures and Magnetic Properties. *Z. Anorg. Allg. Chem.* **2008**, *634*, 2428–2436. [CrossRef]
30. Ferrer, S.; Lloret, F.; Pardo, E.; Clemente-Juan, J.M.; Liu-González, M.; García-Granda, S. Antisymmetric Exchange in Triangular Tricopper(II) Complexes: Correlation among Structural, Magnetic, and Electron Paramagnetic Resonance Parameters. *Inorg. Chem.* **2012**, *51*, 985–1001. [CrossRef] [PubMed]
31. Ferrer, S.; Van Koningsbruggen, P.J.; Haasnoot, J.G.; Reedijk, J.; Kooijman, H.; Spek, A.L.; Lezama, L.; Arif, M.; Miller, J.S. Dimetallic Complexes Derived from a Novel Dinucleating Chelating Symmetric Triazole Ligand; Crystal Structure, Magnetic Properties and ESR Study of Bis[m-3,5-Diacetylamino-1,2,4-Triazolato-O′,N1, N2, O″]Bis[(Nitrato)(Aqua)Copper(II)]. *Dalt. Trans.* **1999**, *23*, 4269–4276. [CrossRef]
32. Li, A.M.; Rentschler, E. 1,2,4-Triazole Schiff Base Directed Synthesis of Polynuclear Iron Complexes: Investigating the Magnetic Properties Going from a Dimer to a 1D Chain to a 3D Framework. *Polyhedron* **2018**, *154*, 364–372. [CrossRef]
33. Liu, Q.; Yao, N.T.; Sun, H.Y.; Hu, J.X.; Meng, Y.S.; Liu, T. Light Actuated Single-Chain Magnet with Magnetic Coercivity. *Inorg. Chem. Front.* **2022**, *9*, 5093–5104. [CrossRef]
34. Sheldrick, G.M. *SADABS, 2014/5*; Bruker AXS Inc.: Madison, WI, USA, 2014.
35. Dolomanov, O.V.; Bourhis, L.J.; Gildea, R.J.; Howard, J.A.K.; Puschmann, H. OLEX2: A Complete Structure Solution, Refinement and Analysis Program. *J. Appl. Crystallogr.* **2009**, *42*, 339–341. [CrossRef]
36. Sheldrick, G.M. SHELXT—Integrated Space-Group and Crystal-Structure Determination. *Acta Crystallogr. Sect. A Found. Adv.* **2015**, *A71*, 3–8. [CrossRef] [PubMed]
37. Sheldrick, G.M. Crystal Structure Refinement with SHELXL. *Acta Crystallogr. Sect. C Struct. Chem.* **2015**, *C71*, 3–8. [CrossRef] [PubMed]
38. Blatov, V.; Shevchenko, A. *ToposPro, Program Package for Multipurpose Crystallochemical Analysis, Version 4.0*; TOPOS: Singapore, 2014.
39. Blanton, J.R.; Papoular, R.J.; Louër, D. PreDICT: A Graphical User Interface to the DICVOL14 Indexing Software Program for Powder Diffraction Data. *Powder Diffr.* **2019**, *34*, 233–241. [CrossRef]
40. Rodríguez-Carvajal, J.; Roisnel, T. Line Broadening Analysis Using Fullprof: Determination of Microestructural Properties. *Mater. Sci. Forum* **2004**, *443–444*, 123–126. [CrossRef]
41. Roisnel, T.; Rodríguez-Carvajal, J. WinPLOT: A Windows Tool for Powder Diffraction Pattern Analysis. *Mater. Sci. Forum* **2001**, *378–381*, 118–123. [CrossRef]
42. Bain, G.A.; Berry, J.F. Diamagnetic Corrections and Pascal's Constants. *J. Chem. Educ.* **2008**, *85*, 532–536. [CrossRef]
43. Neese, F. The ORCA Program System. *Wiley Interdiscip. Rev. Comput. Mol. Sci.* **2012**, *2*, 73–78. [CrossRef]
44. Noodleman, L.; Norman, J.G. The Xα Valence Bond Theory of Weak Electronic Coupling. Application to the Low-Lying States of $Mo_2Cl_8^{4-}$. *J. Chem. Phys.* **1979**, *70*, 4903–4906. [CrossRef]
45. Noodleman, L. Valence Bond Description of Antiferromagnetic Coupling in Transition Metal Dimers. *J. Chem. Phys.* **1981**, *74*, 5737–5743. [CrossRef]
46. Corey, E.J.; Barton, A.E.; Clark, D.A.; Noodleman, L. Electronic Structure of 2-Fe Ferredoxin Models by Xa Valence Bond Theory. *J. Am. Chem. Soc.* **1980**, *102*, 4279–4282.
47. Noodleman, L.; Case, D.A. Density-Functional Theory of Spin Polarization and Spin Coupling in Iron—Sulfur Clusters. *Adv. Inorg. Chem.* **1992**, *38*, 423–458. [CrossRef]
48. Hess, B.A. Relativistic Electronic-Structure Calculations Employing a Two-Component No-Pair Formalism with External-Field Projection Operators. *Phys. Rev. A* **1986**, *33*, 3742–3748. [CrossRef]
49. Ginsberg, A.P. Magnetic Exchange in Transition Metal Complexes. 12.1 Calculation of Cluster Exchange Coupling Constants with the Xα-Scattered Wave Method. *J. Am. Chem. Soc.* **1980**, *102*, 111–117. [CrossRef]
50. Soda, T.; Kitagawa, Y.; Onishi, T.; Takano, Y.; Shigeta, Y.; Nagao, H.; Yoshioka, Y.; Yamaguchi, K. Ab Initio Computations of Effective Exchange Integrals for H-H, H-He-H and Mn_2O_2 Complex: Comparison of Broken-Symmetry Approaches. *Chem. Phys. Lett.* **2000**, *319*, 223–230. [CrossRef]
51. David, G.; Wennmohs, F.; Neese, F.; Ferré, N. Chemical Tuning of Magnetic Exchange Couplings Using Broken-Symmetry Density Functional Theory. *Inorg. Chem.* **2018**, *57*, 12769–12776. [CrossRef]

52. Adamo, C.; Barone, V.; Bencini, A.; Totti, F.; Ciofini, I. On the Calculation and Modeling of Magnetic Exchange Interactions in Weakly Bonded Systems: The Case of the Ferromagnetic Copper(II) M2-Azido Bridged Complexes. *Inorg. Chem.* **1999**, *38*, 1996–2004. [CrossRef] [PubMed]
53. Mukherjee, S.; Gole, B.; Song, Y.; Mukherjee, P.S. Synthesis, Structures, and Magnetic Behavior of a Series of Copper(II) Azide Polymers of Cu_4 Building Clusters and Isolation of a New Hemiaminal Ether as the Metal Complex. *Inorg. Chem.* **2011**, *50*, 3621–3631. [CrossRef] [PubMed]
54. Das, M.; Chattopadhyay, S. Synthesis and Structures of Two Cobalt(III) Complexes with N4 Donor Ligands: Isolation of a Unique Bis-Hemiaminal Ether Ligand as the Metal Complex. *Polyhedron* **2013**, *50*, 443–451. [CrossRef]
55. Ferrer, S.; Hernández-Gil, J.; Valverde-Muñoz, F.J.; Lloret, F.; Castiñeiras, A. Hexanuclear Cu_3O-3Cu Triazole-Based Units as Novel Core Motifs for High Nuclearity Copper(Ii) Frameworks. *RSC Adv.* **2019**, *9*, 29357–29367. [CrossRef] [PubMed]
56. Chilton, N.F.; Anderson, R.P.; Turner, L.D.; Soncini, A.; Murray, K.S. PHI: A Powerful New Program for the Analysis of Anisotropic Monomeric and Exchange-Coupled Polynuclear d- and f-Block Complexes. *J. Comput. Chem.* **2013**, *34*, 1164–1175. [CrossRef] [PubMed]
57. Hu, T.L.; Li, J.R.; Liu, C.S.; Shi, X.S.; Zhou, J.N.; Bu, X.H.; Ribas, J. Syntheses, Crystal Structures, and Magneto-Structural Correlations of Novel CuII Complexes Containing a Planar $[Cu(\mu\text{-}L^1)]_2$(HL^1 = 3-(2-Pyridyl)Pyrazole) Unit: From Dinuclear to Tetranuclear and Then to One-Dimensional Compounds. *Inorg. Chem.* **2006**, *45*, 162–173. [CrossRef] [PubMed]
58. Venegas-Yazigi, D.; Aravena, D.; Spodine, E.; Ruiz, E.; Alvarez, S. Structural and Electronic Effects on the Exchange Interactions in Dinuclear Bis(Phenoxo)-Bridged Copper(II) Complexes. *Coord. Chem. Rev.* **2010**, *254*, 2086–2095. [CrossRef]
59. Gholizadeh Dogaheh, S.; Khanmohammadi, H.; Sañudo, E.C. A New Trinuclear N–N Bridged Cu(II) Complex with an Asymmetric Schiff Base Ligand Derived from Hydrazine. *Polyhedron* **2017**, *133*, 48–53. [CrossRef]
60. Adhikary, A.; Ghosh, K. Fine Tuning of Coordination Environments by Anions on a Series of Cu(II)Dihydrazide Complexes: Syntheses, Structures, Magnetic Properties and Solution Phase Anion Exchange. *Polyhedron* **2019**, *168*, 37–47. [CrossRef]
61. Fan, J.Z.; Du, C.C.; Wang, D.Z. Copper and Manganese Complexes Based on Bis(Tetrazole) Ligands Bearing Flexible Spacers: Syntheses, Crystal Structures, and Magnetic Properties. *Polyhedron* **2016**, *117*, 487–495. [CrossRef]
62. Valero, R.; Illas, F.; Truhlar, D.G. Magnetic Coupling in Transition-Metal Binuclear Complexes by Spin-Flip Time-Dependent Density Functional Theory. *J. Chem. Theory Comput.* **2011**, *7*, 3523–3531. [CrossRef]
63. David, G.; Guihéry, N.; Ferré, N. What Are the Physical Contents of Hubbard and Heisenberg Hamiltonian Interactions Extracted from Broken Symmetry DFT Calculations in Magnetic Compounds? *J. Chem. Theory Comput.* **2017**, *13*, 6253–6265. [CrossRef] [PubMed]